In practice, there is usually a background count N_B. The net peak count $N_{P+B} - N_B = N_{P-B}$ is dependent on the P/B radio as well as on N_{P+B} and N_B separately. The relative error ε_D of the net peak count is

$$\varepsilon_D = \frac{[(N_{P+B}\varepsilon_{P+B})^2 + (N_N\varepsilon_B)^2]^{1/2}}{N_{P-B}}, \qquad (2.3.3.9)$$

which shows that ε_D is similarly influenced by both absolute errors $N_{P+B}\varepsilon_{P+B}$ and $N_B\varepsilon_B$. The absolute standard deviation of the net peak height is

$$\sigma_{P-B} = (\sigma_{P+B}^2 + \sigma_B^2)^{1/2} \qquad (2.3.3.10)$$

and expressed as the per cent standard deviation is

$$\sigma_{P-B} = \frac{(N_{P+B} + N_B)^{1/2}}{N_{P-B}} \times 100. \qquad (2.3.3.11)$$

The accuracy of the net peak measurement decreases rapidly as the peak-to-background ratio falls below 1. For example, with $N_B = 50$, the dependence of σ_{P-B} on P/B is

P/B	σ_{P-B} (%)
0.1	205
1	24.5
10	4.9
100	1.43.

It is obviously desirable to minimize the background using the best possible experimental methods.

2.3.3.7. *Peak search*

The accurate location of the 2θ angle corresponding to the peak of the profile has been discussed in many papers (see, for example, Wilson, 1965). Computers are now widely used for data reduction, thereby greatly decreasing the labour, improving the accuracy, and making possible the use of specially designed algorithms. It is not possible to present a description of the large number of private and commercial programs. The peak-search and profile-fitting methods described below have been successfully used for a number of years and are representative of the results that can now be obtained. They have greatly improved the results in phase identification, integrated intensity measurement, and analyses requiring precise profile-shape determination. It is likely that even better programs and methods will be developed in this rapidly changing field.

There are two levels of the types of data reduction that may be done. The easiest and most frequently used method is usually called 'peak search'. It computes the 2θ angles and intensities of the peaks. The results have good precision for isolated peaks but give the values of the composite overlapping reflections as they appear, for example, on a strip-chart recording. The calculation is virtually instantaneous and is often all that is needed for phase identification, lattice-parameter determination, and similar analyses. The second, profile fitting, described below, is a more advanced procedure that can resolve overlapping peaks into individual reflections and determines the profile shape, width, peak and integrated intensities, and reflection angle of each resolved peak. This method requires a prior knowledge of the profile-fitting function. It is used to determine the integrated intensities for analyses requiring higher precision such as crystal-structure refinement and quantitative analysis, and profile-shape parameters for small crystallite size, microstrain and similar studies.

To measure weak peaks, the counting statistical accuracy must be sufficient to delineate the peak from the background. When the intensity and peak-to-background ratio are low, the computing time is much increased. Since powder patterns often contain a number of weak peaks that may not be required for the analysis, computer programs often permit the user to select a minimum peak height (MPH) and a standard deviation (SD) that the peak must exceed to be included in the data reduction. For example, MPH = 1 would reject peaks less than 1% of the highest peak in the recorded pattern, and SD = 4 requires the intensity to exceed the background adjacent to the peak by $4B^{1/2}$. The number of peaks rejected depends on the intensity and peak-to-background ratio as illustrated in Fig. 2.3.3.7, where the cut-off level was set at $\bar{B} + 4\bar{B}^{1/2}$ for two recordings of the same pattern with about a 40 times difference in intensities. All visible peaks are included in the high-intensity recording and several are rejected by the cut-off level selected in the lower-intensity pattern.

Before carrying out the computer calculations, it may be desirable to subtract unusual background such as is caused by a glass substrate in a thin-film pattern.

The following method was developed using computer-generated profiles having the same shapes as conventional diffractometer (Fig. 2.3.1.3) profiles and adding random counting statistical noise (Huang & Parrish, 1984; Huang, 1988). The best results were obtained using the first derivative ($dx/dy = 0$) of a least-squares-fitted cubic polynomial to locate the peaks, combined with the second derivative ($d^2y/dx^2 =$ minimum) of a quadratic/cubic polynomial to resolve overlapped reflections (Fig. 2.3.3.8). Overlaps with a separate ≥ 0.5 FWHM can be resolved and measured and the accuracy of the peak position is 0.001° for noise-free profiles. Real profiles with statistical noise have a precision of ±0.003 to 0.02° depending on the noise level. The Savitzky & Golay (1964) method (see also Ateiner, Termonia & Deltour, 1974; Edwards & Willson, 1974) was used for smoothing and differentiation of

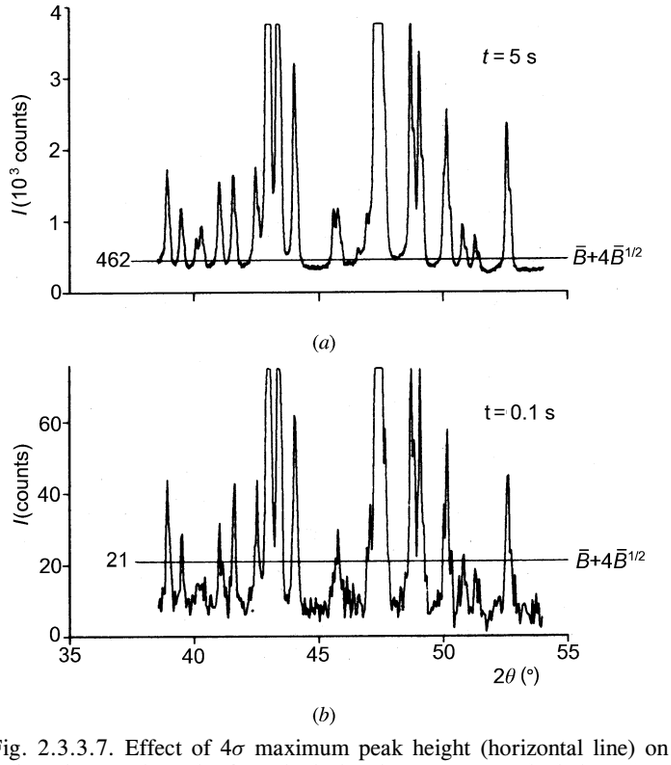

Fig. 2.3.3.7. Effect of 4σ maximum peak height (horizontal line) on dropping weak peaks from inclusion in computer calculation. Step scan with (*a*) $t = 5$ s and (*b*) $t = 0.1$ s. Five-compound mixture, Cu $K\alpha$.

the data by least squares in which the values of the derivatives can be calculated using a set of tabulated integers. The convolution range CR expressed as a multiple of the FWHM of the peak can be selected. A minimum of five points is required. For asymmetric peaks, such as occur at small 2θ's, a CR $\simeq 0.5$ FWHM gives the best precision. The larger the CR the larger the intrinsic error but the smaller the random error, and the smaller the number of peaks identified in overlapping patterns. The larger CR also avoids false peaks in patterns with poor counting statistics. Fig. 2.3.3.8(*c*) shows the dependence of the accuracy of the peak determination on P/σ. The computer results list the 2θ's, d's, absolute and relative intensities (scaled to 100) of the identified peaks. The calculation is made with a selected wavelength such as $K\alpha_1$ and the possible $K\alpha_2$ peaks are flagged.

2.3.3.8. *Profile fitting*

Profile fitting has greatly advanced powder diffractometry by making it possible to calculate the intensities, peak positions, widths, and shapes of the reflections with a far greater precision than had been possible with manual measurements or visual inspection of the experimental data. The method has better resolution than the original data and the entire scattering distribution is used instead of only a few features such as the peak and width. Individual profiles and clusters of reflections can be fitted, or the entire pattern as in the Rietveld method (Chapter 8.6).

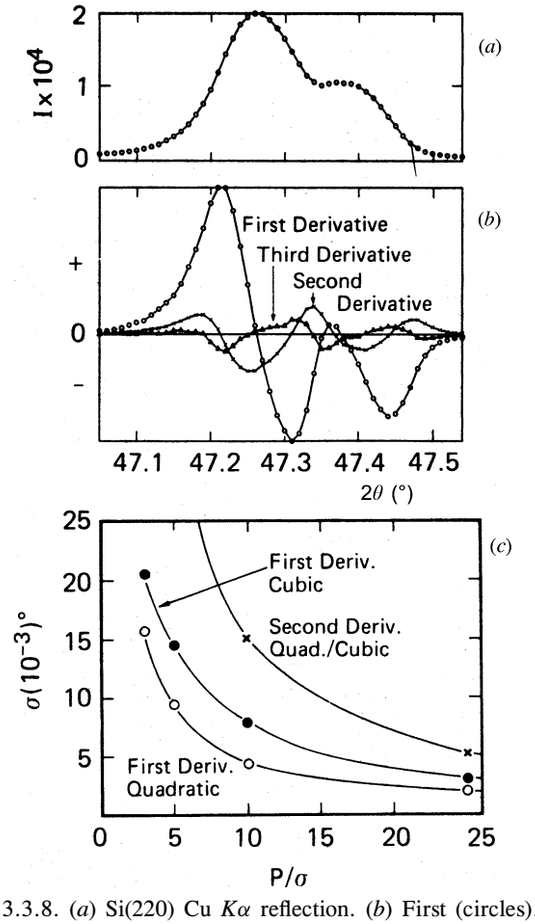

Fig. 2.3.3.8. (*a*) Si(220) Cu $K\alpha$ reflection. (*b*) First (circles), second (crosses), and third (triangles) derivatives of a seven-point polynomial of data in (*a*). (*c*) Average angular deviations as a function of P/σ for various derivatives.

The procedure is based on the least-squares fitting of theoretical profile intensities to the digitized powder pattern. The profile intensity at the ith step is calculated by

$$Y(x_i)_{\rm calc} = B(x_i) + \sum_j I_j P(x_i - T_j)_j, \qquad (2.3.3.12)$$

where $B(x_i)$ is the background intensity, I_j is the integrated intensity of the jth reflection, T_j is the peak-maximum position, $P(x_i)_j$ is the profile function to represent the profile shape, and $\sum_j$ is taken over j, in which the $P(x)_j$ has a finite value at x_i. Unlike the Rietveld method, a structure model is not used. In the least-squares fitting, I_j and T_j are refined together with background and profile shape parameters in $P(x)_j$. Smoothing the experimental data is not required because it underestimates the estimated standard deviations for the least-squares parameters, which are based on the counting statistics.

The experimental profiles are a convolution of the X-ray line spectrum λ and all the combined instrumental and geometrical

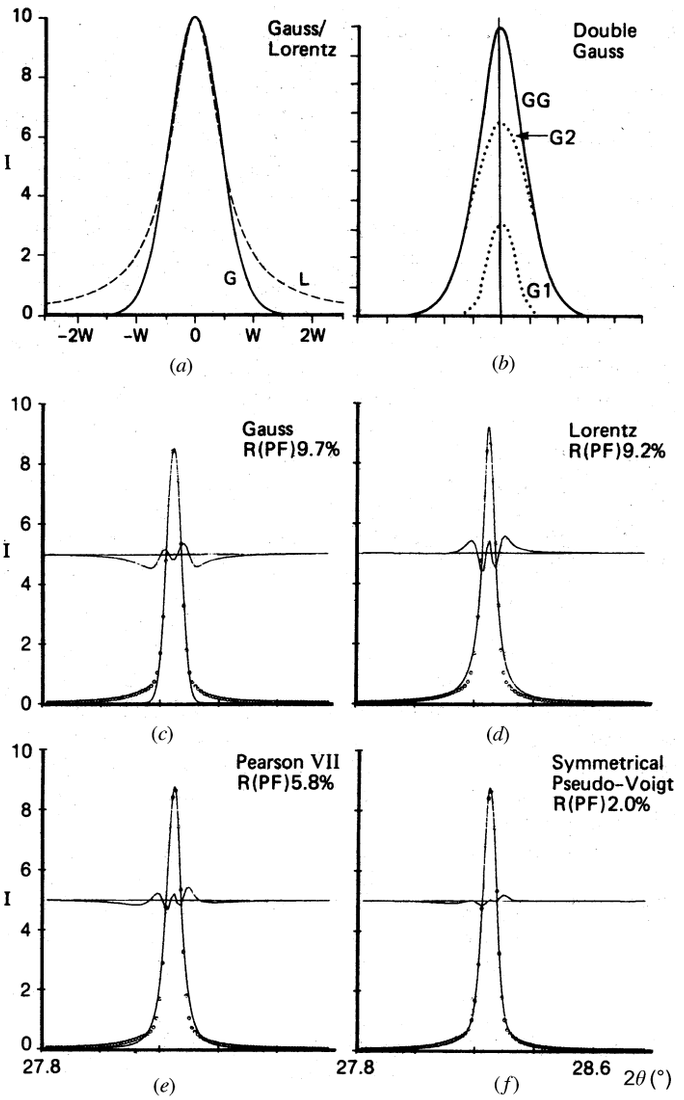

Fig. 2.3.3.9. (*a*) Computer-generated symmetrical Lorentzian profile L and Gaussian G with equal peak heights, 2θ and FWHM. (*b*) Double Gaussian GG shown as the sum of two Gaussians in which I and FWHM of $G1$ are twice those of $G2$ and 2θ is constant. (*c*)–(*f*) Profile fitting with different functions. Differences between experimental points and fitted profile shown at one-half height. Synchrotron radiation, Si(111).

references